Peer-reviewed version available at Water 2019, 11, 132; doi:10.3390/w11010132

Simulation of flow and agricultural non-point source pollutant transport in a Tibetan Plateau irrigation district

Yuqing Li[a], Zuhao Zhou[b*], Kang Wang[c], and Chongyu Xu[c,d]

[a] Tibet Agriculture and Animal Husbandry College, Nyingchi, Tibet, 806000, China;

[b] State Key Laboratory of Simulation and Regulation of Water Cycle in River Basin，China Institute of Water Resources and Hydropower Research Beijing 100038, China;

[c] State Key Laboratory of Water Resources and Hydropower Engineering Science, Wuhan University, Wuhan 430072, China;

[d] Department of Geosciences Hydrology, University of Oslo, Norway

[*]Corresponding author: Phone: +010-68785610, Fax: +010-68785625,

E-mail: zhzh@iwhr.com

Abstract

Flow and transport processes in soil and rock play a critical role in agricultural non-point source pollution (ANSP) loads. In this study, we investigated the ANPS load discharged into rivers from an irrigation district in the Tibetan Plateau, and simulated ANPS load using a distributed model involving detailed descriptions of flow and ANPS transport and transformation processes in the soil and rock. Experiments were conducted for two years to

measure soil water content and nitrogen concentrations and the quality and quantity of lateral flow in the rock and at the drainage canal outlet during the highland barley growing period. A distributed model, in which the subsurface lateral flow was described using a step-wise method, was developed to simulate flow and ammonium nitrogen and nitrate nitrogen transport. Sobol's method was used to evaluate the sensitivity of simulated flow and transport processes to model inputs. The results showed that, with a 21.2% increase of rainfall and irrigation in the highland barley growing period, the average NH_4^+-N and NO_3^--N concentrations in the soil layer decreased by 10.8% and 14.3%, respectively, due to increased deep seepage. Deep seepage of rainfall water accounted for 0–52.4% of total rainfall, whereas deep seepage of irrigation water accounted for 36.6–45.3% of total irrigation. NH_4^+-N and NO_3^--N discharged into the drainage channel represented 19.9–30.4% and 19.4–26.7% of the deep seepage, respectively. The mean Nash-Sutcliffe coefficients, root mean square errors, and cumulative deviations between the measured and simulated flow rates and NH_4^+-N and NO_3^--N concentrations at the surface drainage canal outlet were 0.694, 0.081, and 0.242, respectively, indicating that the proposed method can effectively describe the hydrological and ANPS pollution migration in the plateau irrigation zone. The Sobol' sensitivity analysis results demonstrated that subsurface lateral flow had the most important first order and total effect on the simulated flow and NH_4^+-N and NO_3^--N concentrations at the surface drainage outlet.

Keywords: irrigation zone; Tibetan Plateau; non-point source pollution; Sobol' sensitivity analysis; subsurface lateral flow

1. Introduction

Irrigation areas are the largest contributors to agricultural non-point source (ANPS) pollution in surface and ground water systems (Ibrikci et al., 2015; Jiménez-Aguirre and Isidoro, 2018). Fertilizers, which play a key role in agriculture supplying essential nutrients like nitrogen, are a major non-point source (NPS) pollutant (Marinov and Roelsma, 2005; Meynendonckx et al., 2006; Wang et al., 2014). In recent years, research has focused on the impacts of agricultural land-use management on NPS pollutant migration processes. This information can be employed to simulate NPS pollution processes in irrigation areas using distributed watershed hydrological and NPS pollution models, e.g., CASC2D (Ogden and Julien, 2002), DWSM (Borah et al., 2002), and SWAT (Neitsch et al., 2002; Arnold et al., 2012; Čerkasova et al., 2018), which can effectively model NSP loads (Liu et al., 2017; Franqueville et al., 2018). The modules in these models have been modified to reflect the migration processes of water and fertilizer in irrigation zones. For instance, the soil water and groundwater evaporation module was improved in the SWAT model to reflect the impact of crops on the hydrological cycle (Xie and Cui, 2011). Additionally, the terrain elevation was corrected in the spatial grid unit to describe the irrigation drainage system (Lee et al., 2010; Chahinian et al., 2011).

However, hydrological processes in agricultural irrigation areas are largely influenced by manual irrigation drainage processes. Therefore, the underlying surface conditions and runoff generation and confluence processes in irrigation zones differ significantly different from those in natural watersheds (Lucadamo et al., 2007; Howarth, 2008; Kroeze, 2012; Zhou et al., 2012). Additionally, frequent water exchange exists both inside and outside of the irrigation region (Pollock et al., 2005; Watanabe et al., 2007), which leads to different hydrological mechanisms driving ANPS pollution transport to those of previously mentioned models (Dechmi et al., 2012; Abdelwahab et al., 2018). More importantly, because watershed

hydrological and ANPS pollution models must consider the macroscopic flow properties of the watershed, these models often describe the microscopic soil hydrological processes using relatively simple methods. In agricultural irrigation districts, however, the process of pollutant discharge into a river is mainly influenced by soil hydrological and pollutant migration and transformation processes (Belcher et al., 2004; Wang et al., 2016). As a result, the successful application of these models in complex irrigation and drainage areas remains limited.

An important issue when applying distributed models to simulate ANPS loads in Tibetan Plateau irrigation areas is the physical basis of the subsurface flow and transport and transformation processes. Due to significant differences in their regional conditions and hydrogeological characteristics, ANPS pollution patterns show unique characteristics in these areas. For example, in Nyingchi Prefecture, Tibet, irrigation zones are often located in valley terraces, where the soil layer is commonly as thin as 40–60 cm and underlain by rock comprising loose rubble and sand gravels. Because the soil layer is relatively thin and highly permeable, it is difficult to attain direct surface runoff into rivers under irrigation conditions. ANPS pollution is discharged from the soil into the river through various processes including seepage from soil to rock, subsurface lateral flow in the rock, groundwater flow, and surface drainage, as well as pollution conversion and transport processes. At present, little is known about the migration and transformation of irrigation water after deep seepage into the loose rock medium nor its discharge process into the river or surface drainage canal though subsurface lateral flow in the rock.

A number of parameters and physical variables have been used to describe ANPS pollution transport and transformation in different flow processes from the soil to the drainage canal outlet (Franceschini, 2010). These processes include seepage from soil into rock, subsurface lateral and vertical flow in the rock, and subsurface drainage. Sobol's method is a global sensitivity analysis method that determines the impacts of each parameter and its

interactions with other parameters on the model output (Sobol, 1993; Zhang et al., 2013; Massmann et al., 2014). Previous research has demonstrated the benefits of Sobol's method for identifying different flow and transport processes in models (Nossent et al., 2011; Zhang, et al., 2013). However, it is also crucial to evaluate the use and significance of model parameters.

The objectives of this study are to investigate the effects of subsurface lateral flow and ANPS pollution transport and transformation on the ANPS pollution load discharged from an irrigation district in the Tibetan Plateau into rivers, and to simulate ANPS load using a distributed model including a detailed description of flow and ANPS pollution transport and transformation processes in the soil and rock. The study was conducted in Danniang irrigation district for the major ANPS pollutants of ammonium nitrogen (NH_4^+-N) and nitrate nitrogen (NO_3^--N).

2. Materials and Methods

2.1 Study area

The experiments were conducted in the Danniang irrigation district of Miling, Nyingchi prefecture, Tibet, from May to September in 2014 and 2015. The total and actual irrigated area was 1.28×10^3 hm^2 and 4.26×10^2 hm^2, respectively. Spring highland barley was the main crop planted in this area. From 1953 to 2014, the average annual temperature was 8.7°C and the extreme maximum and minimum temperatures were 32.4°C and -15.3°C, respectively. The annual average relative humidity was 64.2%. The average annual precipitation was 664.5 mm, which was predominantly concentrated from May to September (81.4% of the annual

Preprints (www.preprints.org) | NOT PEER-REVIEWED | Posted: 3 December 2018 doi:10.20944/preprints201812.0025.v1

Peer-reviewed version available at Water 2019, 11, 132; doi:10.3390/w11010132

precipitation). The average annual pan evaporation was 1734.1 mm. The annual average wind speed was 1.68 m/s and the annual average sunshine hours were 2064.6 h.

The irrigation and drainage canals in the irrigation district are shown in Fig. 1. The main irrigation channel was arranged along the contour lines of the piedmont. Sub-irrigation districts 1, 2, 3, 7, and 8 were located in the long and narrow region in the piedmont and irrigated with water directly from the main irrigation channel. Sub-districts 4, 5, and 6 were irrigated with water from the branch irrigations channels. The average elevation difference between the main irrigation channel and drainage channel was 3.6 m.

The soil thickness was 50 cm and underlain with a loose rock layer comprised of coarse sand and rubble 2–40 cm in size. The soil was classified as dark brown soil according to the standards of the second national soil survey in China and sandy loam according to the standards of the US Department of Agriculture (UNSADO). The rock layer was more than 20 m thick. Samples were taken at 12 locations in the irrigation zone to determine soil physical parameters (Table 1). Fertilization was performed twice with a dose of 180.0 and 60.0 kg urea/hm^2 for the first and second irrigation, respectively.

Table 1 Soil physical properties

Depth (cm)	Clay / %		sand / %		silt / %		Bulk density / g/ cm^3
	Mean±STD	Max/Min	Mean±STD	Max/Min	Mean±STD	Max/Min	Max/Min
0-10	12.4±4.3	17.3/10.6	53.6±2.3	55.4/47.0	24.7±4.6	28.6/16.4	0.98/1.32
20-30	12.9±9.6	20.4/10.1	55.0±8.7	57.9/47.4	27.1±0.9	30.0/22.0	1.20/1.42
30-40	10.4±7.7	14.8/9.4	52.3±4.1	61.3/48.2	27.3±3.9	31.0/23.0	1.24/1.48
40-55	11.8±6.3	19.4/7.3	52.4±3.6	54.9/45.6	27.8±5.6	33.8/21.5	1.22/1.38
55~	0	0	100.0±0.0	100/100	0	0	1.36/1.40

2.2 Monitoring hydrological and NPS pollution transport and transformation processes in the soil and rock

Soil samples were taken in different layers (each 10 cm thick) from 0–50 cm depth during the growing period of spring highland barley. The samples were obtained at 12 locations to determine soil water content and concentrations of major NPS nitrogen pollutants

(NH_4^+-N and NO_3^--N). All soil samples were collected using a cutting ring with a volume of 100 cm^3. 14 and 15 sampling events were conducted during the growing period of highland barley in 2014 and 2015, respectively. The soil water content and NH_4^+-N and NO_3^--N concentrations in these samples were measured at the Farmland Water Conservancy Laboratory of the Tibet Agriculture and Animal Husbandry College.

A subsurface lateral flow experimental site was constructed in the irrigation district (Fig. 1) to measure subsurface lateral flow in the rock (Fig. 2). Two 78-m-long and 2-m-wide experimental plots were set up. The plot length was identical to those of ridged fields in the irrigation area. The borders of the experiment plot were isolated with steel plates compressed into the ground to a depth of 20 cm. A 0.5 m-wide protected area was set outside the steel plates, wherein steel plates were arranged in parallel to the experimental plots. Two subsurface lateral flow monitoring sections (A and B) were set at 0.5 m and 20.0 m, respectively, behind the ridge of plots. A working area (5.0 m long, 4.0 m deep, and 2.0 m wide) was excavated mechanically. Subsurface lateral flow collection devices were set at a depth of 3 m below the soil. The collection devices were compressed into the rock to 20 cm depth. A tipping-bucket automatic water recorder was introduced to measure lateral flow rate. The bucket had a volume of 50 mL and automatically tipped after being filled. The time and frequency of tipping were automatically recorded, enabling automatic monitoring of the subsurface lateral flow. The subsurface lateral flux was measured during the growing period of the highland barley. Meanwhile, the lateral flow water was collected to measure NH_4^+-N and NO_3^--N concentrations. The area between sections A and B was covered with a rainproof film to prevent water infiltration into the soil. The amount of irrigation in the experimental area was identical to that in the field during the growing period of highland barley.

The kinetic coefficient of pollutant transformation was determined based on the mass balance method (Shibata, 2011; Urakawa et al., 2014). A stainless-steel sleeve (10 cm long

and 5 cm in diameter) was used for unperturbed sampling in the soil-loose rock medium. Ion exchange resins were placed at the bottom and top of the steel sleeve to eliminate the effects of the in- and out-fluxes of pollutants at the border on the transformation process. The steel sleeve was returned to the sampling point. After the samples were taken around the sampling points, backfilling was conducted in accordance with bulk density. The samples were retrieved 7 d later. The NH_4^+-N and NO_3^--N concentrations were measured during sampling and 7 d later, then the mass difference was taken as the amount of pollutant transformation. During the sowing–tilling, jointing–heading, and flowering–filling stages of the highland barley, samples were taken at three positions in the soil layer (10–40 cm depth) and loose rock layer (70–90 cm depth). The measurements were made twice, three times, and once, respectively, during the three growing stages.

A monitoring section, i.e., section O in Fig. 1, was set at the outlet of the surface drainage canal in the irrigation district. The drainage process was monitored automatically using a Doppler flowmeter, and water samples were taken to measure NH_4^+-N and NO_3^--N concentrations in the surface drainage.

Meteorological parameters (radiation, temperature, humidity, wind speed, and air pressure) were measured at a meteorological station within the study area.

2.3 Simulation of hydrological and NPS pollution migration processes in the plateau irrigation area

Water flow and transport processes were simulated in the sub-irrigation districts with different parameters related to the irrigation events and size of the sub-irrigation district. The flow and pollution fluxes at the outlet of the drainage canal represent the confluence and superposition processes of flow discharged from the rock, including from subsurface lateral flow and groundwater.

A step-wise method was used to describe flow processes in the rock. Subsurface lateral flow in the soil-loose rock medium in the sub-irrigation district is illustrated in Fig. 3. Monitoring data from 2014 and 2015 showed that no significant surface runoff occurred during irrigation. Soil water mainly showed one-dimensional vertical movement. The seepage flux L_i that enters the loose rock layer through the soil layer was calculated based on the water balance relationship. In the interval i–i+1, the seepage flux L_i that enters the loose rock medium through the soil layer can be expressed as

$$L_i = I - \Delta W_i \quad (1)$$

where I is the amount of irrigation (or rainfall) and ΔW_i is the variation of soil water content before and after irrigation (or rainfall). ΔW_i was calculated as follows: (field water holding capacity - soil water content at the beginning of irrigation) × depth of soil layer.

In the soil and loose rock medium, the impact of the diffusion process on pollutant migration can be ignored in the case of a long seepage path, and the convection (the product of water flow flux and concentration) process can be used to describe the pollutant migration flux. Given the complex transformation process of nitrogen in soil, the measured values of nitrogen concentration in the soil layer were taken as the model's input for the calculation. The mean values of the measured soil water content and NH_4^+-N and NO_3^--N concentrations in the soil profile were used in the calculation.

The flux L_i seeps into the loose rock medium through the soil layer and moves (laterally) toward to the surface drainage canal as well as vertically into the groundwater. In the interval from section i-1 to section i, the lateral inflow flux at section i is denoted as S_i (Fig. 3b). In the interval from section i to section i+1, only a partial flux of S_i continuously moves to the surface drainage canal due to high arbitrariness of flow in the loose fractured medium. At section i+1, the lateral flow flux S_i decreases to $S_{i,i+1}$. At section i, the lateral flux to the surface drainage canal is the superposition of all fluxes. Similarly, the flux at section i+1 includes

lateral flow from soil seepage, denoted as flux S_{i+1}, and the total lateral flow migrated into the interval at section i. The total subsurface lateral flow flux in the loose rock medium at section i can be expressed as

$$S = \sum_{j=0}^{m} S_{i-j,i} \quad (2)$$

The relationship between the subsurface lateral flux at the two adjacent sections can be expressed as

$$S_{i,i+1} = S_i \mu(G) \quad (3)$$

A subsection-fitting method was used for calculation of the subsurface lateral flow coefficient $\mu(G)$ in the loose rock medium (Wang et al., 2013),

$$\mu(G) = \alpha e^{-\beta t} \sqrt{t} \quad (4)$$

where t is the relative time (seepage time/irrigation duration) and α and β are parameters related to the rock structure.

The methods describing the pollutant transformation process in porous media are generally summarized as kinetic and lumped methods (Hansen, 1991, Wang et al., 2014). The kinetic method describes the transformation process of pollutants under the effects of various physical, chemical, and biological processes (Wang et al., 2016), whereas the lumped method describes the collective transformation processes of pollutants (Wang et al., 2014). In this study, we combined the above two methods and used the lumped first-order kinetic coefficient to describe the attenuation of ANPS pollutant concentration under the combined effects of various physical, chemical, and biological processes:

$$c_{t+1} = c_t e^{-kt} \quad (5)$$

where c_t and c_{t+1} are the concentrations of pollutants (NH_4^+-N and NO_3^--N) seeping out at times t and t+1 (mg/L) and k is the lumped first-order kinetic coefficient (d^{-1}).

The amount of leached water from the soil to the aquifer in the section from i to i+1 is

Preprints (www.preprints.org) | NOT PEER-REVIEWED | Posted: 3 December 2018 doi:10.20944/preprints201812.0025.v1

Peer-reviewed version available at Water 2019, 11, 132; doi:10.3390/w11010132

$$wr_{i,i+1} = S_i(1-\mu(G)) \tag{6}$$

Assuming that variations in groundwater flow are linearly related to the rate of change in water table height, we obtain:

$$\frac{dQ_{gwi,i+1}}{dt} = \frac{K_s}{\mu L_g^{\,2}}(wr_{i,i+1} - Q_{gwi,i+1}) \tag{7}$$

where $Q_{gwi,i+1}$ is the groundwater flow into the surface drainage canal, μ is the specific yield of the shallow aquifer (cm^3/cm^3), and L_g is the distance from the ridge of the groundwater to the surface drainage canal. Water flow and chemical transport processes in the drainage canal can be characterized by the following equations:

$$\frac{\partial A}{\partial t} + \frac{\partial\left(Q^2/A\right)}{\partial x} + gA\left(\frac{\partial h}{\partial x} - R_0 + R_f\right) = S \tag{8}$$

$$Q = \frac{A}{n}R^{2/3}R_f^{1/2} \tag{9}$$

where A is the cross-sectional area of the drainage channel, Q is the cross-sectional flow rate, S is the unit inflow for the calculation period, as determined using Eqs. (2) and (7), h is the depth of the drainage channel, n is the Manning roughness coefficient, R and R_0 are the hydraulic radius and longitudinal slope of the drainage channel, respectively, and R_f is the friction slope. Due to the prevention of field ridges and the high soil permeability in the irrigation zone, irrigation and rainfall did not typically produce runoff.

2.4 Calibration of model parameters

Parameters related to subsurface lateral flow in the rock, groundwater flow, and surface drainage were calibrated based on the monitored flow rates, NH_4^+-N concentration, and NO_3^--N concentration at sections A and B in the rock and at the outlet of the drainage canal. The objective function was defined as

$$\Phi([b]) = \sum_{j=1}^{m_q} v_j \sum_{i=1}^{n_{qj}} \left(g_j^*(x,t_i) - g_j(x,t,[b]) \right)^2 \quad (10)$$

where m_q is the number of monitoring variables (flux, NH_4^+-N concentration, and NO_3^--N concentration), n_{qj} is the monitoring number of variable j, $g_j^*(x,t_i)$ is the monitored value of variable j at time t_i in the monitoring position, and $g_j(x,t_i,[b])$ is the result of using optimized parameter [b]. Additionally, v_j is the weight of variable j, which is used to reduce the magnitude effect of different variables and different monitoring events on the calculated results:

$$v_j = \frac{1}{n_j \sigma_j} \quad (11)$$

where σ_j is the standard deviation of the monitored value for variable j.

The hydrological process in each sub-irrigation district was simulated using Eqs. (3) and (4). By taking the subsurface and groundwater outflow process as the source-sink term in the surface drainage channel, the flow rate process in the surface drainage channel was simulated using Eqs. (8) and (9). The pollutant migration flux in the drainage channel was based on simulation of the convection process, and the pollutant transformation process in the river was simulated using Eq. (5).

The simulation results of the NH_4^+-N and NO_3^--N concentrations were evaluated using four indicators: the Nash-Sutcliffe coefficient (NSE) (Nash and Sutcliffe, 1970), the relative root mean square error (*rRMSE*), the relative deviation (F_B), and the relative total error (F_E)(ISO,1993). NSE, F_B, and F_E are denoted as

$$NSE = 1 - \frac{\sum_{t=1}^{n} (O_t - P_t)^2}{\sum_{i=1}^{n} (O_t - \bar{O})^2} \quad (12)$$

$$F_B = \frac{1}{n} \sum_{i=1}^{n} \frac{P_t - O_t}{(P_t + O_t)/2} \quad (13)$$

$$F_E = \frac{1}{n}\sum_{i=1}^{n}\frac{|P_t - O_t|}{(P_t + O_t)/2} \quad (14)$$

where O_t and P_t are the monitored and calculated values at time t, respectively, $\bar{O}$ is the mean of the monitored value, and n is the number of observation points. The ideal value of NSE was 1. F_B and F_E were used to describe the systematic error and total deviation between the observed and simulated values.

2.5 Sobol' sensitivity analysis

The effects of input parameters on model performance were evaluated using the Sobol' method. The model can be represented in the following functional form

$$Y = f(X) = f(x_1, x_2 \ldots x_n) \quad (15)$$

where Y is the model output and X=(x_1, x_2,…x_n) is the parameter and physical variable set. For all of parameters and physical variables used in the model, two low difference random sequences are generated using the random sampling method.

$$M_A = \begin{bmatrix} x_{11} & x_{12} & \cdots & x_{1n} \\ x_{21} & x_{22} & \cdots & x_{2n} \\ \vdots & \vdots & \vdots & \vdots \\ x_{m1} & x_{m2} & \cdots & x_{mn} \end{bmatrix} \quad M_B = \begin{bmatrix} x'_{11} & x'_{12} & \cdots & x'_{1n} \\ x'_{21} & x'_{22} & \cdots & x'_{2n} \\ \vdots & \vdots & \vdots & \vdots \\ x'_{m1} & x'_{m2} & \cdots & x'_{mn} \end{bmatrix} \quad (16)$$

where m is the sampling repetition and n is the number of parameters. A new matrix was formed by replacing the parameters in the i-th column in matrix B; i.e., sample values of parameter X_i, with the i-th column data in matrix A.

Preprints (www.preprints.org) | NOT PEER-REVIEWED | Posted: 3 December 2018 doi:10.20944/preprints201812.0025.v1

Peer-reviewed version available at Water 2019, 11, 132; doi:10.3390/w11010132

$$M_{C_i} = \begin{bmatrix} x_{11} & x_{12} & \cdots & x'_{1i} & \cdots & x_{1n} \\ x_{21} & x_{22} & \cdots & x'_{2i} & \cdots & x_{2n} \\ \vdots & \vdots & \vdots & \vdots & \vdots & \vdots \\ x_{m1} & x_{m2} & \cdots & x'_{mi} & \cdots & x_{mn} \end{bmatrix} \quad i=1, 2\ldots n \qquad (17)$$

Finally, matrices A and B were vertically stacked into one "combined" matrix, C, which has n+2 rows and n columns. The first order sensitivity index, S_i, and the total order sensitivity index, S_{Ti}, were calculated as follows:

$$S_i = \frac{\frac{1}{m-1}\sum_{k=1}^{m} y_B^{(k)} y_C^{(k)} - \frac{1}{m}\sum_{k=1}^{m} y_A^{(k)} y_B^{(k)}}{V(y_A)} \qquad (18)$$

$$S_{Ti} = 1 - \frac{\frac{1}{m-1}\sum_{k=1}^{m} y_B^{(k)} y_C^{(k)} - \left(\frac{1}{m}\sum_{k=1}^{m} y_A^{(k)}\right)^2}{V(y_A)} \qquad (19)$$

where $y_A^{(k)}$, $y_B^{(k)}$, and $y_C^{(k)}$ are the model outputs with parameters in matrices A, B, and C, respectively. The variance of the output with the parameters in matrix A is calculated as:

$$V(y_A) = \frac{1}{m-1}\sum_{k=1}^{m}\left(y_A^{(k)} - \frac{1}{m}\sum_{k=1}^{m} y_A^{(k)}\right)^2 \qquad (20)$$

The first order index, S_i, is a measure of the variance contribution of the individual parameter X_i to the total model variance. The difference between the first order sensitivity index and the total order sensitivity index can be regarded as a measure of the interaction between parameter X_i and the other parameters.

3. Results and Discussion

3.1 Characterization of flow and NH_4^+-N and NO_3^--N transport

Figs. 4(a) and (b) show the distribution of NH_4^+-N and NO_3^--N concentrations, respectively, in the soil profile during the highland barley growing season in 2014. Figs. 4(c) and (d) show the same distributions for 2015. The total rainfall and irrigation were 712 mm and 863 mm for the growing period of highland barley in 2014 and 2015, respectively. Compared with the mean NH_4^+-N and NO_3^--N concentrations in the soil profile in 2014, the mean NH_4^+-N concentration decreased by 14.22%, 11.47%, and 6.78%, respectively, and the mean NO_3^--N concentration in the soil layer decreased by 3.18%, 22.4%, and 17.3%, respectively, for the sowing–tilling, jointing–heading, and flowering–filling stages of 2015. Due to a 21.2% increase in rainfall and irrigation in the 2015 period, the average concentrations of NH_4^+-N and NO_3^--N decreased in the soil layer by 10.8% and 14.3%, respectively. In the bottom soil layer (40–50 cm), the peak concentrations of NH_4^+-N and NO_3^--N for 2014 were 0.86 and 4.08 mg/L, respectively, whereas, for 2015, these concentrations were 0.65 and 3.76 mg/L, representing a decrease of 24.4% and 7.8%, respectively.

Figs. 5 (a)–(c) compare the rainfall and irrigation, subsurface lateral flow rate per unit width, and NH_4^+-N and NO_3^--N concentrations in subsurface lateral flow, monitored at the lateral flow experimental site during the two growing periods. Table 2 compares the deep seepage fluxes (i.e., seepage fluxes from the soil to the loose rock layer) of NH_4^+-N and NO_3^--N measured during each growth stage. For the three irrigation events in 2014 (Fig. 5a), the amount of deep seepage water entering the rock layer through the soil accounted for 37.4%, 36.6%, and 41.2% of the irrigation, respectively. For 2015, deep seepage accounted for 40.2%, 45.3%, and 39.4% of the irrigation, respectively. Deep seepage due to rainfall accounted for 0–52.4% of all rainfall.

Table 2. Comparison of NH_4^+-N and NO_3^--N mass seepage rates per area (g/s/hm^2) during the highland barley growing periods.

	Sowing and tillering stages		Jointing and heading stages		Flowering and paddle stages	
	Mean	Max/Min	Mean	Max/Min	Mean	Max/Min
2014						

NH_4^+-N	6.14×10^{-5}	$9.78\times10^{-5}/3.30\times10^{-5}$	4.24×10^{-5}	$1.01\times10^{-4}/1.77\times10^{-5}$	2.11×10^{-5}	$8.94\times10^{-5}/1.57\times10^{-5}$
NO_3^--N	3.25×10^{-5}	$5.14\times10^{-5}/1.07\times10^{-5}$	3.44×10^{-4}	$5.78\times10^{-4}/1.21\times10^{-4}$	8.60×10^{-5}	$1.84\times10^{-4}/3.39\times10^{-5}$
2015						
NH_4^+-N	7.44×10^{-5}	$1.26\times10^{-4}/0.54\times10^{-5}$	3.99×10^{-5}	$7.93\times10^{-5}/1.15\times10^{-5}$	2.02×10^{-5}	$4.64\times10^{-5}/1.33\times10^{-5}$
NO_3^--N	3.18×10^{-5}	$8.74\times10^{-5}/2.21\times10^{-5}$	4.04×10^{-4}	$6.48\times10^{-4}/2.04\times10^{-4}$	7.54×10^{-4}	$1.02\times10^{-3}/5.48\times10^{-4}$

The peak concentration of NH_4^+-N in subsurface lateral flow in the rock appeared after fertilization in both 2014 and 2015. Overall, at Section A, the NH_4^+-N concentration decreased over the growing period of highland barley. Compared with the flow rate and NH_4^+-N and NO_3^--N concentrations at Section A in 2014, the mean value of the flow rate and NH_4^+-N and NO_3^--N concentrations at Section B decreased by 34.2%, 54.8%, and 44.6%, respectively, and the peak values decreased by 82.4%, 44.2%, and 38.7, respectively. With increased rainfall and irrigation in 2015, the difference in flow rate and pollution concentrations between Section A and B decreased; the mean value of the flow rate and NH_4^+-N and NO_3^--N concentrations at position B only decreased by 24.2%, 34.5%, and 28.7%, respectively, and the peak values only decreased by 74.4%, 24.2%, and 14.7, respectively.

As shown in Fig. 5, during periods of less rainfall, such as June and July in 2014 and June in 2015, the flow peaks at Section B lagged behind the flow peaks at position A due to water storage in rock pores and fractures. Compared with Section A, the NH_4^+-N and NO_3^--N concentrations at Section B decreased in both years. NH_4^+-N decreased by 34.2% and 22.4% in 2014 and 2015, respectively, while NO_3^--N decreased by 12.4% and 8.3%.

3.2 Simulation of NPS pollutant migration and transformation processes

The calibrated parameters are listed in Table 3. Figs. 6 (a)–(c) compare the simulated and measured flow rate and NH_4^+-N concentration and NO_3^--N concentration at the outlet (Section

Preprints (www.preprints.org) | NOT PEER-REVIEWED | Posted: 3 December 2018 doi:10.20944/preprints201812.0025.v1

Peer-reviewed version available at Water 2019, 11, 132; doi:10.3390/w11010132

O) of the surface drainage canal. With increasing rainfall and irrigation, lateral flow was greatly affected by the amount of deep seepage, resulting in a deviation of the simulation results. This also indicates differences in the peak value and mechanism of NH_4^+-N and NO_3^--N pollutant concentrations, as well as in the peak value and mechanism of flow rate in the loose rock medium. As shown in Fig. 6, the flow rates simulated with the calibrated parameters were lower than the values measured in July 2015. The mean values of the measured and simulated flow rates were 0.0338 m^3/s and 0.0402 m^3/s at the outlet of the drainage canal. Soil seepage into the rock was significantly reduced because rainfall was only 14.5 mm in June 2015 (Fig. 4) and part of the seepage was stored in fractures and pores in the rock instead of discharged into the surface drainage canal. As a result, the model underestimated flow rates and overestimated NH_4^+-N and NO_3^--N concentrations by 4.71% and 5.64% for this period.

Table 3
Parameter and physical variable list

No.	Brief descript (unit)	Process	Calibrated	Minimum	Maximum
1	Seepage from soil into rock (mm/d), *LE*	Soil		1.4	12.6
2	NH_4^+-N concentration in the soil water(mgL^{-1})	Soil		0.4	6.2
3	NO_3^--N concentration in the soil water(mgL^{-1})	Soil		1.8	8.4
4	α, Parameter in Eq.2,	subsurface lateral flow	1.554	1.00	2.05
5	β, Parameter in Eq.2,	subsurface lateral flow	0.0182	0.0020	0.110
6	NH_4^+-N decay rate in the lateral flow in the rock(d^{-1})	subsurface lateral flow	0.142	0.102	0.20
7	NO_3^--N decay rate in the lateral flow in the rock(d^{-1})	groundwater	0.171	0.144	0.224
8	K_{sat} ,Parameter in Eq. 5($m\ s^{-1}$),	groundwater	3.42×10^{-5}	3.08×10^{-5}	3.94×10^{-5}
9	μ ,Parameter in Eq. 6,	groundwater	0.15	0.12	0.18
10	*L* ,Parameter in Eq. 7 (m),	groundwater	240	200	280
11	NH_4^+-N decay rate In the surface drainage(d^{-1})	Surface drainage	0.11	0.09	0.14
12	NO_3^--N decay rate In the surface drainage (d^{-1})	Surface drainage	0.09	0.06	0.13

Table 4 Model performance evaluation

	NSE	r_{RMSE}	F_E	F_B
Flow rate	0.791	5.132	0.2014	0.031
NH_4^+-N concentration	0.701	8.364	0.2466	0.048

NO_3^-N concentration	0.644	7.532	0.3172	-0.051

At the outlet of the drainage canal, two NH_4^+-N concentration peaks were observed after the first fertilization. The NH_4^+-N concentration peak after second fertilization was only slightly higher than the NH_4^+-N concentration before fertilization (Fig. 6). Although the second fertilization amount was significantly less than the first fertilization amount, the difference in transport processes from soil to drainage canal in the various sub-irrigation districts was attributed more to the difference in pollution concentrations between in the soil and the outlet of the drainage canal. Over the entire growing period of highland barley, the NH_4^+-N concentration at the outlet of the drainage canal was 1.37 times the mean NH_4^+-N concentration of the soil profile. Conversely, the NO_3^--N concentration scope was 0.88 times the mean NO_3^--N concentration of the soil profile. This result indicates that the impacts of transformation processes within the rock on the pollution load were significant.

F_B remained less than 5% throughout the growing period of highland barley, demonstrating no systematic error between the simulated and measured results. F_B and F_E of the simulated values were within the range of ±0.15/0.3 (F_B/F_E), indicating high accuracy of the simulation. All the results of the Nash-Sutcliffe coefficient, *rRMSE*, and F_E demonstrate that the model can effectively describe the migration and transformation processes of pollutants in the soil-loose rock medium and their fluxes into the river in this plateau irrigation area.

Table 5 shows the simulation results of subsurface lateral flow rate per unit width from the porous medium to the drainage channel, the mass of NH_4^+-N and NO_3^--N in deep seepage from the soil into the loose rock medium, the mass of NH_4^+-N and NO_3^--N pollutants transformed in the soil-loose rock medium, and the mass of NH_4^+-N and NO_3^--N entering the discharge channel through seepage. During the growing period of highland barley in 2015, 29.4% of deep seepage water was due to irrigation and rainfall discharged into the drainage

Preprints (www.preprints.org) | NOT PEER-REVIEWED | Posted: 3 December 2018 doi:10.20944/preprints201812.0025.v1

Peer-reviewed version available at Water 2019, 11, 132; doi:10.3390/w11010132

channel. The transformation of NH_4^+-N accounted for 13.0–22.4% of total NH_4^+-N in deep seepage, whereas NH_4^+-N discharge into the drainage channel accounted for 19.9–30.4% of total NH_4^+-N in deep seepage. The transformation of NO_3^--N accounted for 11.2–14.1% of total NO_3^--N in deep seepage, whereas NO_3^--N discharge into the drainage channel accounted for 19.4–26.7% of total NO_3^-N in deep seepage.

Table 5 Mass balance of non-point source pollutions during the hihland barley growing periods

Growing stages	Lateral seepage /10^4m^3/km	NH_4^+-N mass / 10^1kg/km			NO_3^--N mass / 10^1kg/km		
		Deep leaching	Transformation process	Pollution discharged into river	Deep leaching	Transformation process	Pollution discharged into river
Sowing and tillering stages	2.16	2.55	0.571	0.774	4.38	0.491	0.977
Jointing and heading stage	3.64	2.386	0.329	0.642	8.42	1.190	2.245
Flowering and paddle stage	3.87	0.492	0.064	0.098	7.45	0.977	1.442
Total	9.67	5.428	0.964	1.514	20.25	2.658	4.664

3.3 Sensitivity evaluation of model parameters

It is noted that the sum of all first order indices is less than 1, which means that the model is in-additive, as expected. Flow and NH_4^+-N and NO_3^-- N transport simulations are sensitive to the variations of α and β in Eq. (2). It is clear that the α and β in Eq. (2) is the most important parameter. The sensitivity index of □ is the highest in all flow and NH_4^+-N and NO_3^--N transport processes. Additionally, flow and NH_4^+-N and NO_3^-- N transport simulations are sensitive to the variations of α and β in Eq. (2). The first- and total-order sensitivity indices of 12 parameters are shown in Fig. 7. The x-axis represents the parameter number listed in Table 3 and the y-axis represents the first- and total- order sensitivity indices (black and gray bars, respectively). Regarding the flow and NH_4^+-N and NO_3^--N transport processes, the first- and total- order sensitivity indices of the parameters related to lateral surface flow in the rock (α and β) were significantly higher than the other parameters. The first- and total- order sensitivity indices of the parameters related to groundwater discharge

into surface drainage were the lowest of all parameters. These results were attributed to the lower discharge of water, NH_4^+-N, and NO_3^-- N from groundwater than from subsurface lateral flow.

The parameters related to lateral surface flow exhibited the maximum sensitivity. Regarding NH_4^+-N transport from the soil to the surface drainage outlet, the value of S_i for soil NH_4^+-N concentration was higher than the rates of flow seepage from the soil into the rock. The difference in S_i and S_{Ti} values for the NH_4^+-N decay coefficient in lateral surface transport and surface drainage transport was significantly higher than the differences between other parameters. The results also showed that 65.2% of the variations in the simulated NH_4^+-N concentrations at the surface drainage outlet were caused by variations of α and β in Eq. 2 and 18.4% of the variations were attributed to the decay of NH_4^+-N. Although the values of α and β in Eq. (2) were the most sensitive parameters in the NO_3^-- N transport simulation, the values decreased by 45.2% and 27.2% compared to the values of α and β in the flow and NH_4^+-N simulations, respectively. The sensitivity of NO_3^--N concentrations in the soil was also lower than that of NH_4^+-N concentrations in the soil.

4. Conclusions

Field experiments were conducted to investigate the hydrology and ANPS pollutant migration and transformation processes in the Danniang irrigation region, Tibet, during the growing seasons of highland barley in 2014 and 2015. A distributed model was constructed to simulate flow and ANPS pollution (NH_4^+-N and NO_3^--N) transport and transformation from the soil to the outlet of the drainage canal. Water flow and transport processes were simulated in sub-irrigation districts with different parameters related to the irrigation events and the size of the sub-irrigation districts. A step-wise method was used to describe subsurface lateral flow in the rock. The flow and pollution fluxes at the outlet of the drainage canal represented the

confluence and superposition processes of flow discharged from the rock, including subsurface lateral flow and groundwater.

The simulated values of flow rate, NH_4^+-N concentration, and NO_3^--N concentration exhibited systematic deviations of less than 15%. Across the growing period of highland barley, the mean values of the Nash-Sutcliffe coefficient, *rRMSE*, and cumulative deviation between the simulated and observed flow rates and NH_4^+-N and NO_3^--N concentrations at the outlet of the surface drainage canal were 0.694, 0.081, and 0.242, respectively. These indicate that the proposed method can effectively simulate the hydrological and NPS pollutant migration processes in this plateau irrigation district. As a result of the 21.2% increase of rainfall and irrigation amount in the 2015 growing period of highland barley, the average NH_4^+-N and NO_3^--N concentrations in the soil layer decreased by 10.8% and 14.3%, respectively, due to increased deep seepage. Deep seepage due to rainfall accounted for 0–52.4% of all rainfall, whereas deep seepage due to irrigation accounted for 36.6–45.3% of all irrigation. NH_4^+-N and NO_3^--N discharge into the drainage channel represented 19.9–30.4% and 19.4–26.7% of the deep seepage, respectively. Parameters in the subsurface lateral flow simulation were shown to have the most important first order and total effect on the simulated flow and NH_4^+-N and NO_3^--N concentrations at the outlet of the surface drainage channel.

Acknowledgement

This work was partly supported by grants from the National Key Research and Development Program of China (2016YFC0402405), and the National Natural Science Foundation of China (Nos. 91647109, 51679257, 51879195).

References

Abdelwahab, O. M. M., Ricci, G. F., De Girolamo, A. M., Gentile, F.2018. Modelling soil erosion in a Mediterranean watershed: Comparison between SWAT and AnnAGNPS models. Environmental Research, 166: 363-376.

Arnold, J.G., Moriasi, D.N., Gassman, P.W., Abbaspour, K.C., White, M.J., Srinivasan,R., Santhi, C., Harmel, R.D., van Griensven, A., Van Liew, M.W., Kannan, N., Jha,M.K., 2012. SWAT: model use, calibration, and validation. Trans. ASABE 55 (4), 1491–1508.

Belcher, K.W., M.M. Boehm, and M.E. Fulton. Agroecosystem sustainability: a system simulation model approach. Agricul. Sys. 2004. 79:225-241.

Borah, D.K., Xia, R., Bera, M., 2002. DWSM - A dynamic watershed simulation model. Chapter 5 in Mathematical Models of Small Watershed Hydrology and Applications, 113-166. V.P. Singh and D.K. Frevert, eds. Highlands Ranch, Colo.: Water Resources Publications.

Čerkasova, N. Umgiesser, G., Ertürk, A. 2018. Development of a hydrology and water quality model for a large transboundary river watershed to investigate the impacts of climate change – A SWAT application. Ecological Engineering, 124:99-115.

Chahinian N, Tournoud M G, Perrin J L. 2011. Flow and nutrient transport in intermittent rivers: a modelling case-study on the Vene River using SWAT 2005. Hydrological Sciences, 192, 143-159.

Dechmi, F., Burguete, J., Skhiri A. 2012. SWAT application in intensive irrigation systems: Model modification, calibration and validation. Journal of Hydrology, 470–471:227-238.

Franceschini, S., Christina W. Tsai. 2010. Assessment of uncertainty sources in water quality modeling in the Niagara River. Advances in Water Resources, 33, 493–503.

Franqueville, D., Benhamou, C., Pasquier, C., Hénault, C., Drouet, J. L. 2018. Modelling reactive nitrogen fluxes and mitigation scenarios on a landscape in Central France. Agriculture, Ecosystems & Environment, 264: 99-110.

Hansen, S., H.E. Jensen, N.E. Nielsen, and H. Svendsen. 1991. Simulation of nitrogen dynamics and biomass production in winter wheat using the Danish simulation model DAISY. Fert. Res., 27, 245-259.

Howarth, R.W., 2008. Coastal nitrogen pollution: a review of sources and trends globally and regionally. Harmful Algae 8, 14–20.

Ibrikci, H., Cetin, M., Karnez, E. Flügel, W. A., Ryan, J. 2015. Irrigation-induced nitrate losses assessed in a Mediterranean irrigation district. Agricultural Water Management, 148:223-231.

ISO. 1993. Guide to the expression of uncertainty of measurements,Geneva.

Jiménez-Aguirre, M. T, Isidoro, D. 2018. Hydrosaline Balance in and Nitrogen Loads from an irrigation district before and after modernization. Agricultural Water Management, 208: 163-175

Lee S, Yoon C., Jung, Kwang W. 2010. Comparative evaluation of runoff and water quality using HSPF and SWMM. Water Science and Technology, 62(6), 1401-1409.

Liu, R., Wang, Q., Xu, F., Men, C., Guo L. 2017. Impacts of manure application on SWAT model outputs in the Xiangxi River watershed. Journal of Hydrology, 555: 479-488

Lucadamo, L., De Filippis, A., Mezzotero, A., Vizza, S., Gallo, L., 2007. Biological and chemical monitoring of some major Calabrian (Italy) Rivers. Environmental Monitoring and Assessment 146, 453–471.

Kroeze, C., Bouwman, L., Seitzinger, S., 2012. Modeling global nutrient export from watersheds. Curr. Opin. Environ. Sustain. 4, 195–202.

Marinov, D.Q., Roelsma, J., 2005. Simulation of water flow and nitrogen transport for a Bulgarian experimental plot using SWAP and ANIMO models. J. Contam. Hydrol. 77, 145–164.

Massmann, C., Wagener, T., Holzmann, H., 2014. A new approach to visualizing time-varying sensitivity indices for environmental model diagnostics across evaluation time-scales. Environ. Model. Software 51, 190-194.

Meynendonckx, J.,Heuvelmans, G.,Muys, B., Feyen, J., 2006. Effects of watershed and riparian zone characteristics on nutrient concentrations in the River Scheldt Basin. Pap. Hydrol. Earth Syst. Sci. 3, 653–679.

Nash, J. E. Sutcliffe, J. V. 1970. River flow forecasting through conceptual models, Part I - A discussion of principles, Journal of Hydrology 10, 282–290.

Neitsch, S.L., Arnold, J.G., Kiniry, J.R., Srinivasan, R., Williams, J.R., 2002. Soil and Water Assessment Tool User's Manual Version 2000. GSWRL Report 02-02; BRC Report 02-06; TR-192. College Station, Texas: Texas Water Resources Institute.

Nossent, J., Elsen, P., Bauwens, W., 2011. Sobol' sensitivity analysis of a complex environmental model. Environ. Model. Softw. 26 (12), 1515–1525.

Ogden, F.L., Julien, P.Y., 2002. CASC2D: A two-dimensional, physically based, Hortonian hydrologic model. Chapter 4 in Mathematical Models of Small Watershed Hydrology and Applications, 69-112. V.P. Singh and D.K. Frevert, eds. Highlands Ranch, Colo.: Water Resources Publications.

Pollock D. W., R. S. Kookana, and R. L. Correll. 2005. Integration of the pesticide impact rating index with a geographic information system for the assessment of pesticide impact on water quality. Water, Air, & Soil Pollut., Focus, 5: 67-88.

Sobol, I.M., 1993. Sensitivity estimates for nonlinear mathematical models. Math. Model. Comput. Exp. 1 (4), 407–417.

Shibata H., R. Urakawa, H. Toda, Y. Inagaki, R. Tateno. 2011. Changes in nitrogen transformation in forest soil representing the climate gradient of the Japanese archipelago, J For Res, 16:374–385.

Wang, K., Zhang, R., and Sheng, F., 2013. Characterizing heterogeneous processes of water flow and solute Transport in soils using multiple tracer experiments. Vadose Zone Journal, doi:10.2136/vzj2012.0125.

Wang, K, Zhang, R., Chen, H., 2014. Drainage-process analyses for agricultural non-point-source pollution from irrigated paddy systems, Journal of Irrigation and Drainage Engineering, DOI:10.1061/(ASCE)IR.1943-4774. 0000662.

Wang, K., Lin, Z., Zhang, R., 2016. Impact of phosphate mining and separation of mined materials on the hydrology and water environment of the Huangbai River basin, China, Science of the Total Environment. 543, 347–356.

Watanabe T., M. Kimura, and S. Asakawa. 2007. Dynamics of methanogenic archaeal communities based on rRNA analysis and their relation to methanogenic activity in Japanese paddy field soils. Soil Biol. Biochem., 39:2877-2887.

Urakawa R., H. Shibata, M. Kuroiwa. 2014. Effects of freeze thaw cycles resulting from winter climate change on soil nitrogen cycling in ten temperate forest ecosystems throughout the Japanese archipelago, Soil Biology & Biochemistry, 74:82-94

Xie, X., Cui, Y., 2011. Development and test of SWAT for modeling hydrological processes in irrigation districts with paddy rice. Journal of Hydrology 396, 61–71.

Zhang, A., Zhang, C., Fu, G., Wang, B., Bao, Z., Zheng, H., 2012. Assessments of impacts of climate change and human activities on runoff with SWAT for the Huifa River Basin, Northeast China. Water Resour. Manage. 26 (8), 2199–2217.

Zhou, T., Wu, J.G., Peng, S.L., 2012. Assessing the effects of landscape pattern on river water quality at multiple scales: a case study of the Dongjiang River watershed, China. Ecol. Indic. 23, 166–175.

Figure List

Peer-reviewed version available at Water 2019, 11, 132; doi:10.3390/w11010132

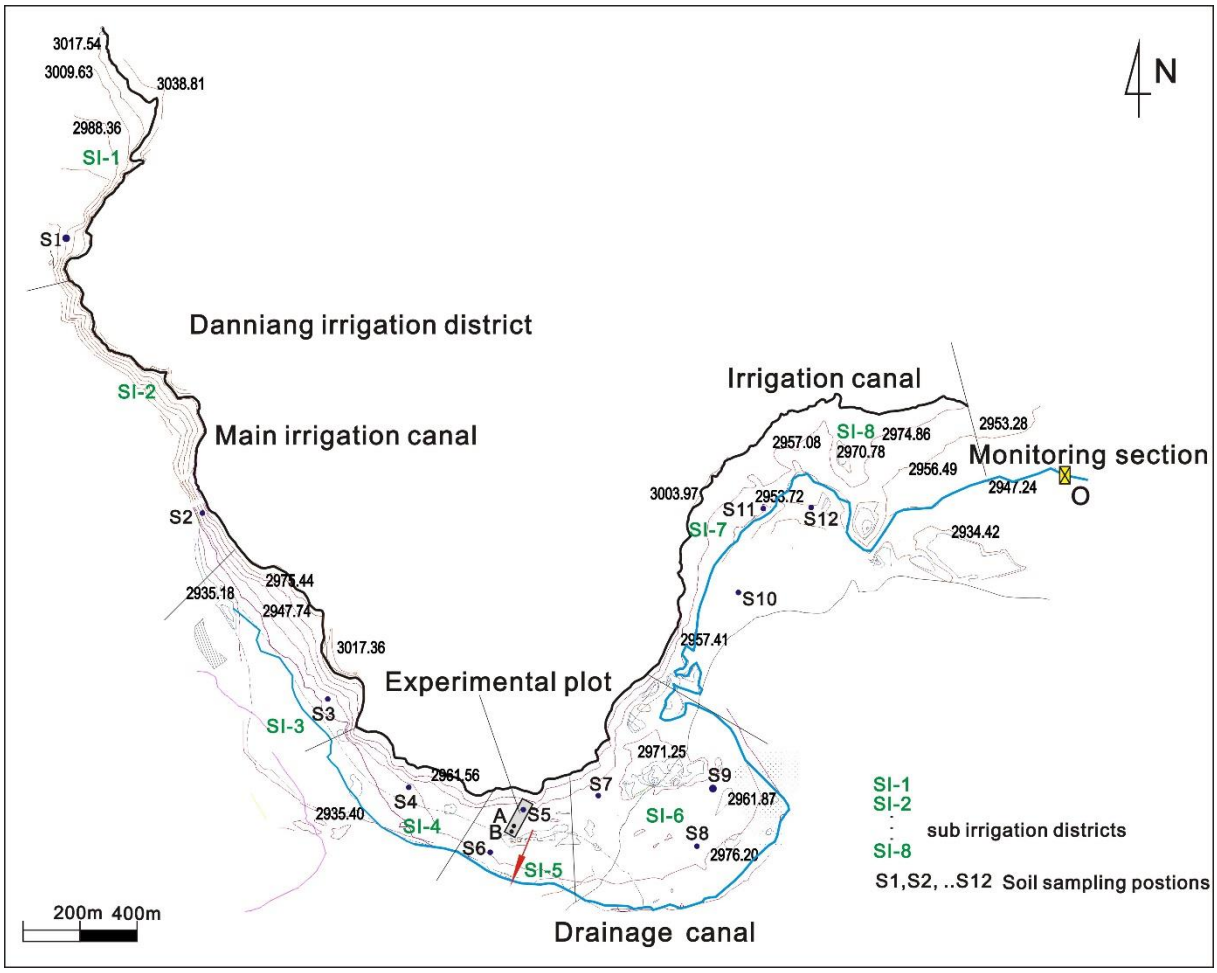

Figure 1

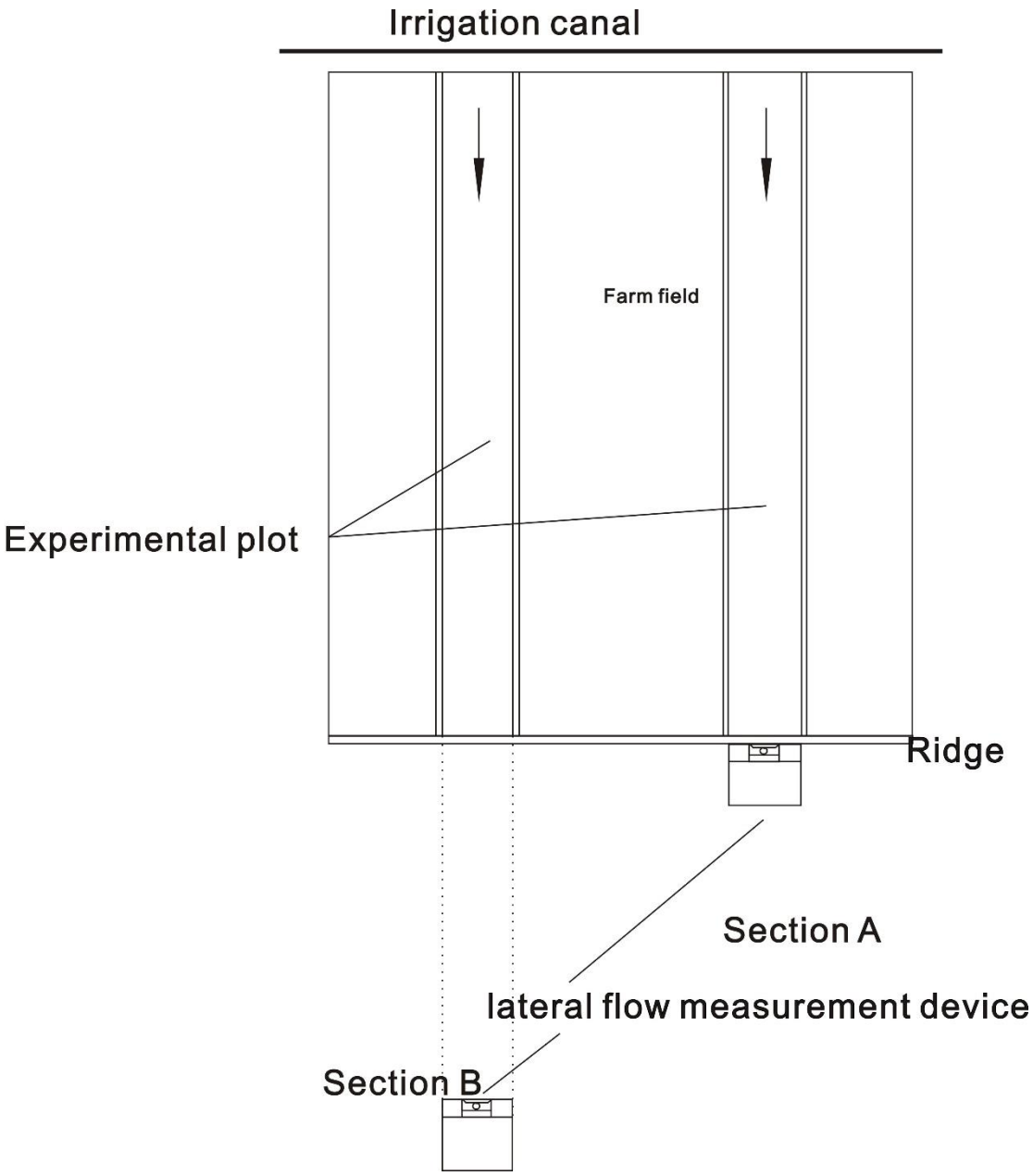

Figure 2

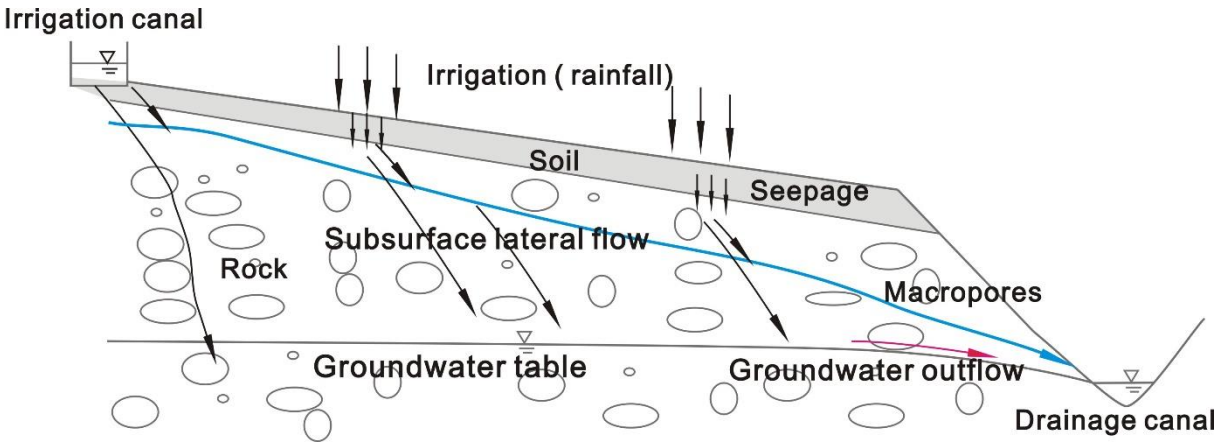

(a)

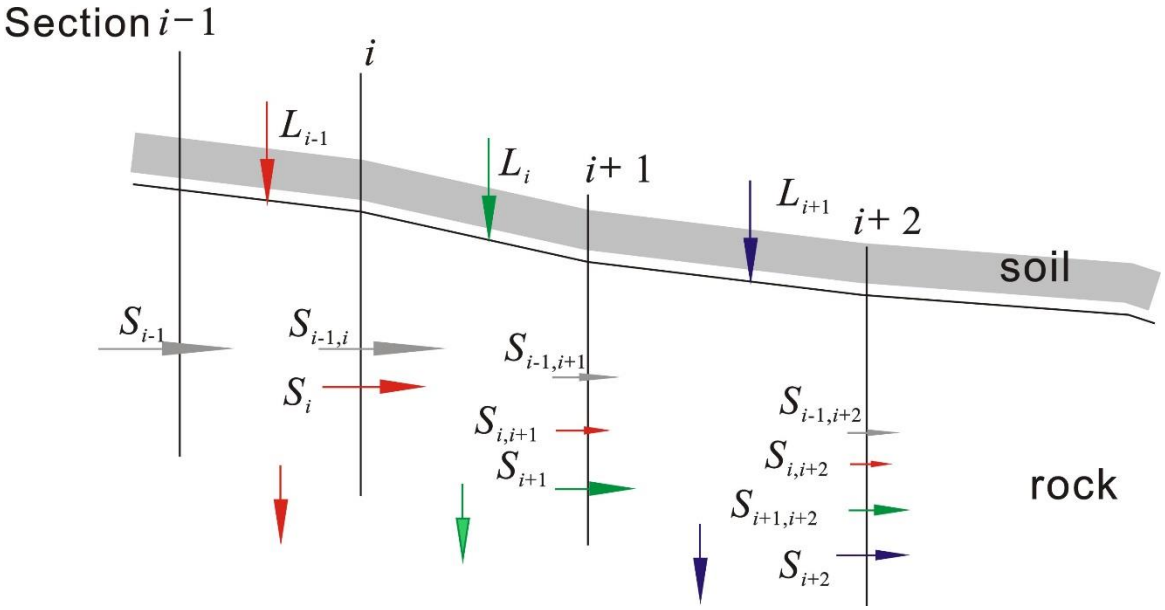

(b)

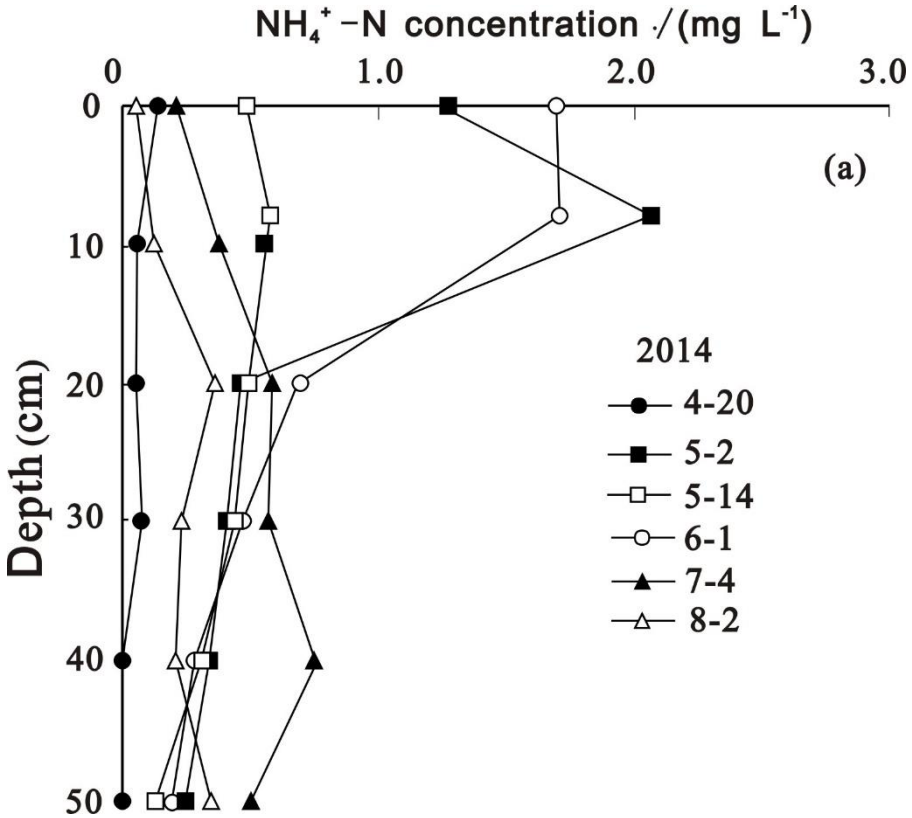

Figure 3

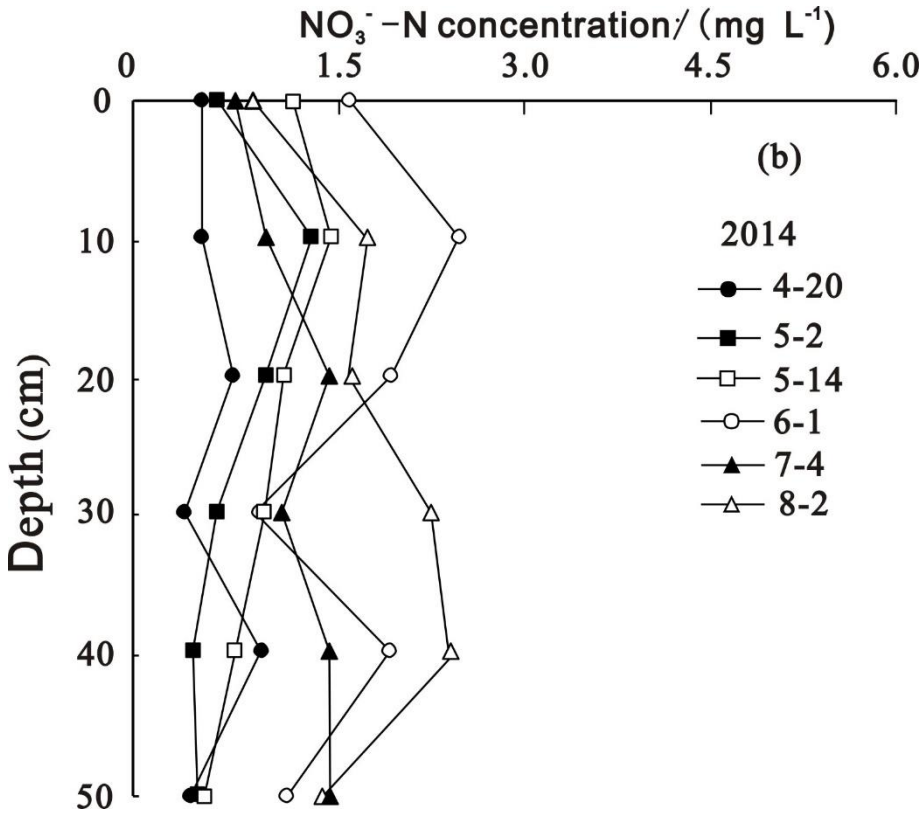

Figure 4

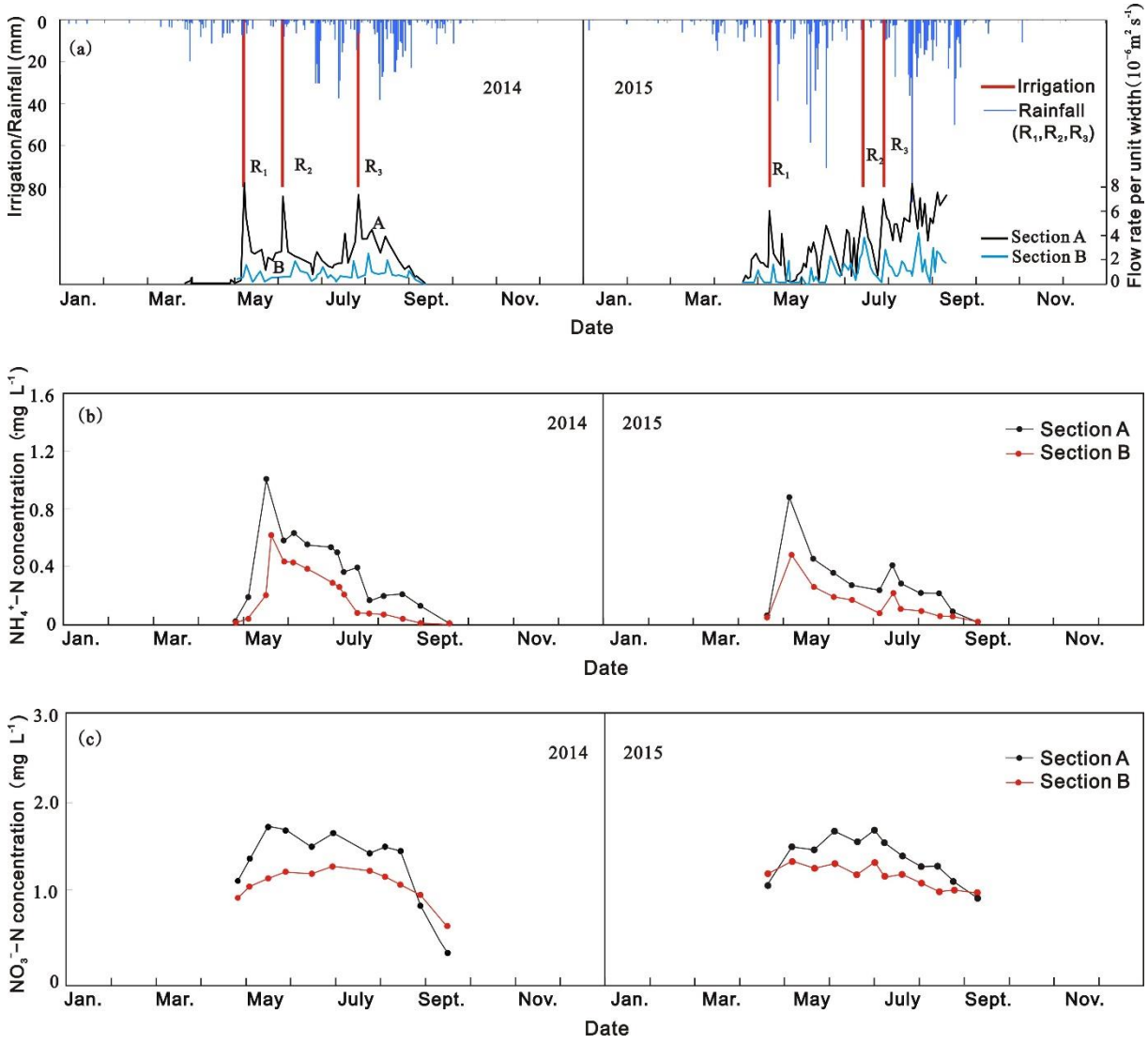

Figure 5

5

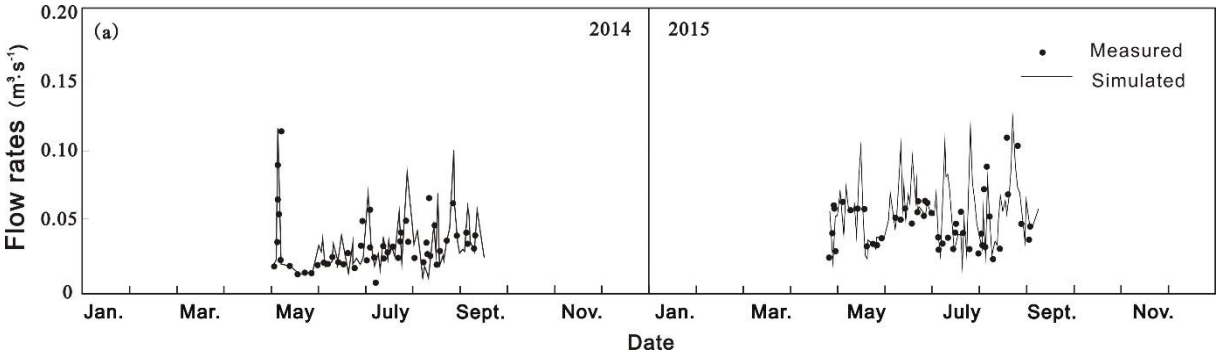

6

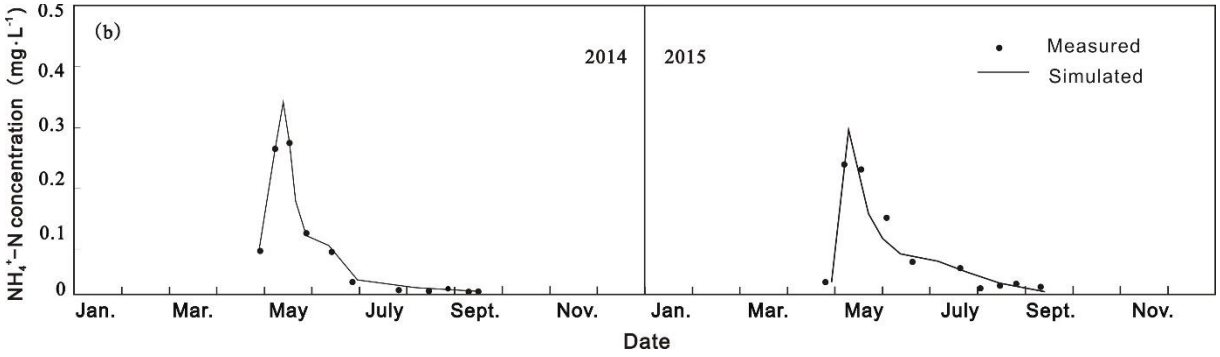

7

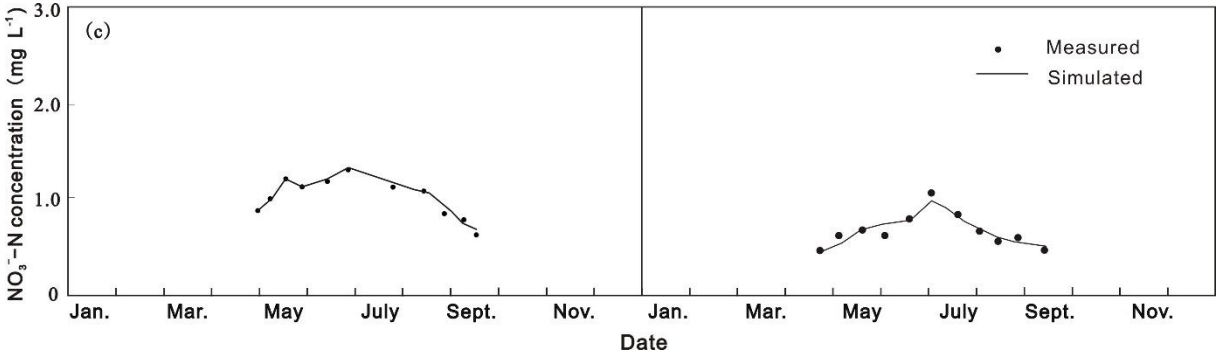

8

9 Figure 6

10

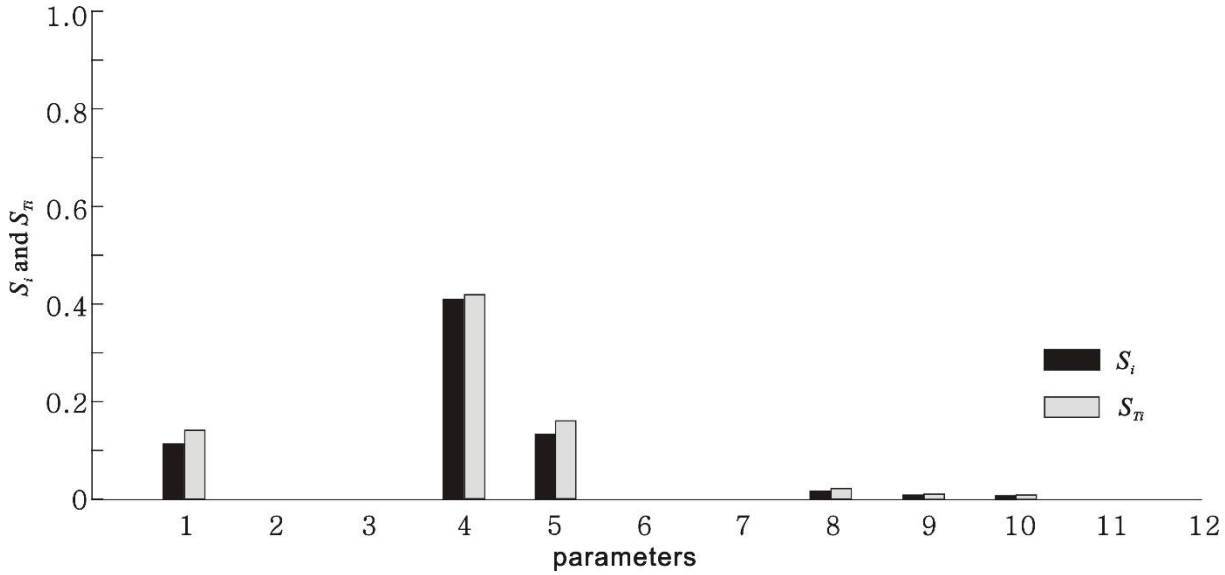

(a) Simulation of flow

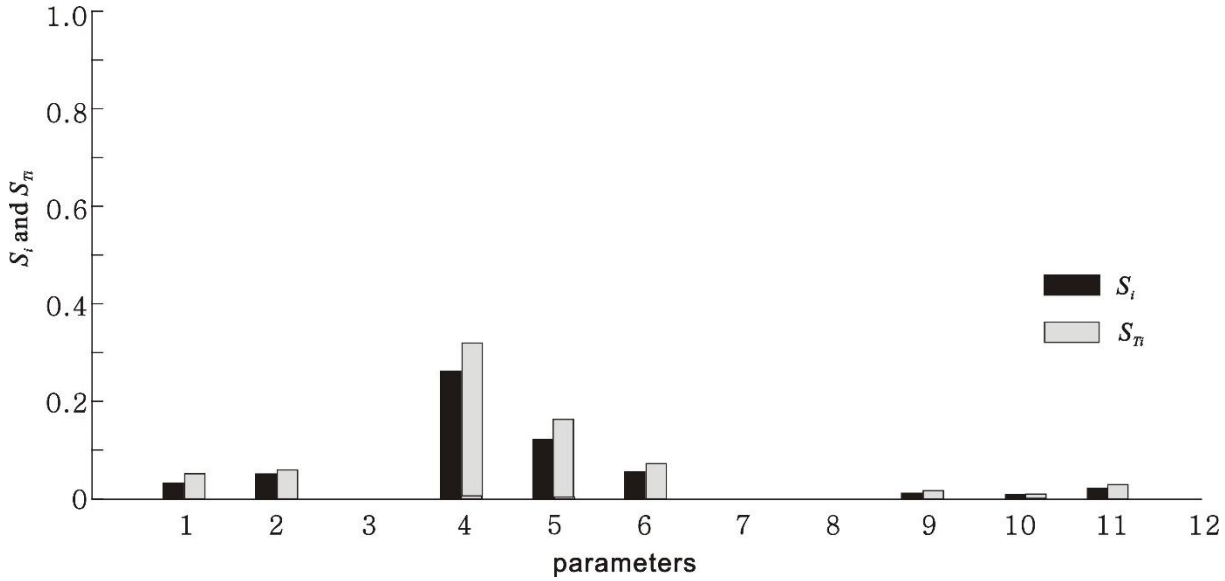

(b) Simulation of NH_4^+-N concentration

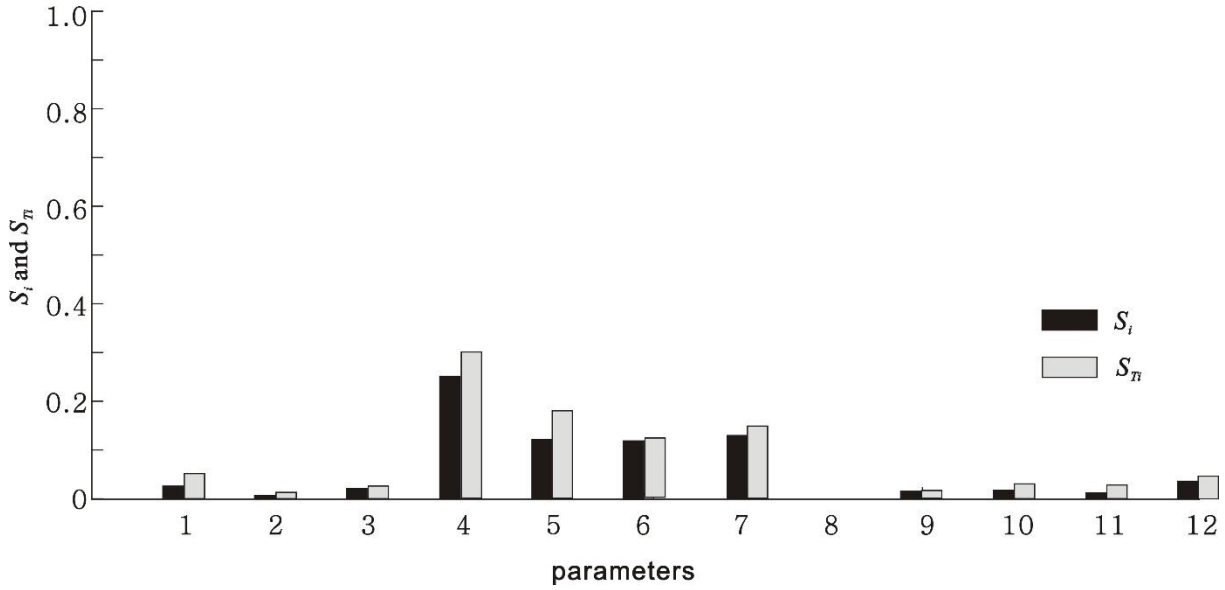

(c) Simulation of NO_3^--N concentration

Figure 7